International Journal of Innovative Computing, Information and Control
Volume **17**, Number **2**, April **2021**

ICIC International ©2021 ISSN 1349-4198
pp. 411–424

THEORETICAL VIBRATION ANALYSIS ON RADIAL VASCULAR MECHANICAL MODELING WITHIN EXPERIMENTAL RESULTS FOR STENOSIS SUBJECTS

Jieyi Zhu[1,*], Meiyan Feng[2] and Guofu Lian[2]

[1]School of Electronic, Electrical Engineering and Physics
[2]School of Mechanical and Automotive Engineering
Fujian University of Technology
No. 33, South Xuefu Road, University Town, Fuzhou 350118, P. R. China
myfeng@fjut.edu.cn; gflian@mail.ustc.edu.cn; *Corresponding author: 19892172@fjut.edu.cn

Received October 2020; revised February 2021

Abstract. *This paper conducts analysis on the human beings' radial artery natural vibration in a micro scale. The radial artery is one important organ in the arterial system. In order to analyze the radial artery vessel, we undertake a three-dimensional modal analysis of the coupled radial-blood system. The radial artery consists of three layers: intima, media, and adventitia. We deduced the theoretical expression of the radial artery mechanical model, and then conducted the theoretical analysis and simulation of radial artery vibration. We considered the normal condition and the varicose condition respectively of the radial artery vascular, comparing the two conditions from both deduction and vibration simulation by finite element method. Lastly the vibration frequencies and vibration mode shapes for each condition were represented for medial analytical applications and solutions. Finally the theoretical simulation is compared with the experimental results obtained from stenosis subjects in order to reveal the inherent relationship. The theoretical analysis and hemodynamics analysis could provide guidance for medical instrument development.*

Keywords: Modal analysis, Radial arterial wall, Stenosis analysis, Waveform analysis

1. **Introduction.** In decades, the study of cardiovascular research became increasingly meaningful in the research of cardiovascular diseases. There have been several kinds of research about cardiovascular system, including the aortic-radial waveform signal analysis, the mechanical modeling of aortic-radial vascular system, and hemodynamics monitor analysis. In the macro level analysis, the radial artery waveforms can be easily obtained by an applanation tonometry instrument, applying an Omron HEM-7012 on the radial artery of the left arm. Based on this medical sensor we could conduct much research in cardiovascular field, such as waveform morphology analysis and transfer function construction. The most classic one is radial-carotid transfer function modeling, as both time domain methods or frequency techniques could be used for estimation [1]. The techniques of fast Fourier transformation could be able to provide more accurate estimation for the radial-aortic calculation [2]. The other kind is the biomechanics analysis for blood vessels or capillaries. For mechanical modeling, we consider the radial vascular vessel as a single hollow micro-cylindrical tube, with blood flowing inside the channel. The highest fluid pressure in the channel is the systolic pressure of the blood as it flows through the radial artery. The lowest pressure of this same blood is the diastolic pressure during one cycle. Although there are some numerical techniques efficient for solving complex partial equations such as element free methods [3], we deduce the explicit formulation of the

DOI: 10.24507/ijicic.17.02.411

relationship between blood pressure and vascular elasticity from present simple hemodynamic model [4]. Fluid-structure interaction is also necessary for mechanical simulation when analyzing the effects of blood pressure on the radial vascular vessel. Ansys software is applicable for this fluid-structure simulation.

Varicose veins have become one ordinary vascular disease for elderly people, as previous studies reported that varicose veins affect approximately 25 percent of the adult population, and complications arising from them leading to a significant cause of patient morbidity and health service expense [5]. From the micro level mechanism, the varicose veins are veins becoming enlarged and twisted [6]. The varicose veins case usually happens in the legs and lower limbs of the patients [7], while in our study in order to conduct our research in a small range, we choose the radial artery for varicose veins study. In our biomechanics study, we conducted the radial vessel mechanical model derivation, comparing the two models between the normal condition and the varicose veins condition. Secondly, the varicose veins' influence was represented in vibration analysis, within the blood-radial vascular interaction on the coupled natural frequencies [8]. Analytical method, based on the modal decomposition, and numerical method, was based on the finite element method [9]. For this purpose, analytical solutions of the problem were obtained and the sensitivity of these natural frequencies and mode shapes were investigated with regards of the layer distribution [10]. The blood was assumed compressible. The vibration frequencies at each mode were demonstrated in a comparison of the normal and the varicose veins conditions. In order to obtain the inherent relationship between radial vascular vibrations with stenosis, we also conducted experiments for a group of subjects including stenosis subjects. We analyzed the realistic pulse waveforms of both stenosis subjects and normal subjects, and summarized the theoretical deduction by the assistance of experimental results.

In summary, in this paper we conducted theoretical analysis for radial vascular modeling of stenosis subjects and normal subjects respectively. The vibration mode analysis and the experimental waveform comparisons are methods and means for theoretical induction to understand vascular stenosis. For practical significance, the theoretical analysis and hemodynamics analysis could provide guidance for developing medical instruments including arterial stiffness detector and hematology analyzer.

2. **Radial Vessel Mechanical Model and Vibration Mode Analysis.** To analyze the theoretical relationship between blood pressure and radial artery viscocity-elasticity strain/stress, it is necessary to examine the radial artery mechanical model. If we consider the blood behavior in a radial segment of a human artery as a one-dimensional, Newtonian, incompressible fluid flow inside an elastic tube, we can deduce the flow quantity expression from a continuity equation:

$$\frac{\partial Q}{\partial z} + \frac{\partial A}{\partial t} = 0 \tag{1}$$

where A is the cross-sectional area, Q is a flow (volume/time) through the elastic tube, and z is the axial direction. According to Bergman et al. [11], the pulsatile flow of an incompressible fluid in a rigid, straight circular cylinder is considered a system of the Cauchy equation of motion reduction:

$$\rho \frac{\partial u}{\partial t} = -\frac{\partial P}{\partial z} + \frac{1}{r}\frac{\partial (rT)}{\partial r} \tag{2}$$

In this equation, ρ is the fluid density, u is the axial velocity of the flowing fluid, P is the dynamic pressure of the flowing fluid, r and z are the radial and axial coordinates respectively, t is the calculus time for computing physical variables' changes over time,

TABLE 1. The mechanical parameters of the three-layer radial vessel model

	E (Pa)	ρ (kg/m^3)	ν	R (m)
Fluid		1000		0.0105
Intima	385643	1150	0.45	0.0107
Media	1156928	1150	0.45	0.0119
Adventitia	385643	1150	0.45	0.0125

and T is the shear stress in the axial direction. And the parameters of the radial vascular vessel are listed in Table 1.

In Table 1, the aorta is composed of three morphologically distinct layers: the intima, media, and adventitia, separated by internal and external elastic laminae. Adventitia is the outer layer of a blood vessel. Media is the middle layer of a blood vessel, and intima is the inner layer or lining of a blood vessel. E, R, ν and ρ stand for Young modulus, radius, poison ratio and density of each layer.

For expressing the shear stress in a rheological model, T is a function of the strain rate in a Newtonian model, and the viscosity μ is therefore regarded as the absolute viscosity, so T can be deduced in (3):

$$T = \mu \frac{\partial u}{\partial r} \tag{3}$$

We use Equation (3) to replace the T in Equation (2), and the linearized momentum equation is given in (4):

$$\rho \frac{\partial u}{\partial t} = -\frac{\partial P}{\partial z} + \mu \left(\frac{\partial^2 u}{\partial r^2} + \frac{1}{r} \frac{\partial u}{\partial r} \right) \tag{4}$$

If the model is under the condition where the radial and tangential motion of fluid is neglected, the pressure gradient can be expressed as the form in Equation (5):

$$-\frac{\partial P}{\partial z} = P_0 \cdot e^{i\omega t} \tag{5}$$

Combining the three Equations (1), (2), and (5) into a joining equation, we obtain the solution, which is already represented in Womersley's paper [12], and is shown in (6):

$$u = u(r, z, t) = \frac{A}{i\omega\rho} \left[1 - \frac{J_1 \left(i^{1.5} \alpha y \right)}{J_0 \left(i^{1.5} \alpha \right)} \right] e^{i\omega t} \tag{6}$$

In this solution $\alpha = (\omega\rho/\mu)^{0.5} r_0$, $y = r/r_0$, r_0 is the internal arterial radius, J_0 and J_1 are zero and first order, respectively, from the Bessel functions of the first kind. Following the above formula derivation, we can create a schematic diagram for the radial artery configuration, shown in Figure 1. Figure 1 represents the model of radial artery vascular, the red cylinder inside stands for the blood flowing in the vessel, and the grey cylinder outside stands for the artery wall. Figure 1 also marks the radial coordinate r and the axial coordinate z, which is used in Equation (2). This figure could be able to describe the rigid model of the radial artery mechanical modeling. This model is an ideal model for radial artery mechanical analysis. However, if we want to consider the blood as flowing stream, the model needs to be modified as a fluid-structure model. In the latter part of this chapter, we would discuss the fluid model.

Considering the fluid model in the bloodstream, the flow in this study is assumed to be laminar Newtonian, viscous, and incompressible. The blood flow is governed by the Navier-Stokes equations of incompressible flow blood on a moving domain [13]. Combining

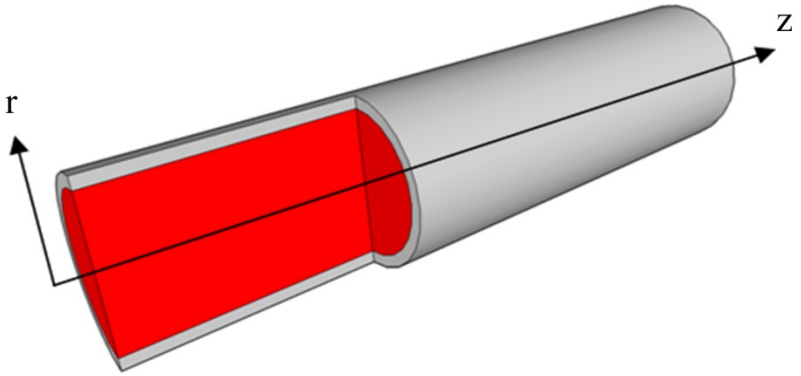

FIGURE 1. The schematic diagram for radial artery configuration

the Navier-Stokes equations and the continuity equations, the governing equations are shown in Equations (7) and (8):

$$\frac{\partial \overrightarrow{V}}{\partial t} + \overrightarrow{V} \cdot \overrightarrow{\nabla} \overrightarrow{V} + \frac{\overrightarrow{\nabla} P}{\rho} - 2\frac{\eta}{\rho} \overrightarrow{\nabla} \cdot D = \overrightarrow{0} \tag{7}$$

$$\nabla \cdot \overrightarrow{V} = 0 \tag{8}$$

where V is the fluid velocity, P is fluid pressure, ρ is density, η is dynamic viscosity, $\overrightarrow{\nabla}$ is the gradient operator and D is the fluid rate of deformation tensor. In that case, in order to analyze the longitudinal vibration and the torsional vibration, the scalar components of the displacements vector u could be expressed by

$$u_r^{(i)} = \frac{\partial \phi_i}{\partial r} + \frac{n}{r}\psi_i - k_z \frac{\partial \chi_i}{\partial r} \tag{9}$$

$$u_\theta^{(i)} = \frac{nk_z}{r}\chi_i - \frac{n}{r}\phi_i - \frac{\partial \psi_i}{\partial r} \tag{10}$$

$$u_z^{(i)} = k_z \phi_i + k_{\psi_i}^2 \chi_i \tag{11}$$

In Equation (9), Equation (10) and Equation (11), the radial wave number (k_{ϕ_i}, k_{ψ_i}) are related to the axial wave number k_z by $k_{\phi_i}^2 = \omega^2/c_{L_i}^2 - k_z^2$, $k_{\psi_i}^2 = \omega^2/c_{T_i}^2 - k_z^2$. ω denotes the angular frequency.

The stress tensor in the arterial layers is given by Hooke's law in terms of potentials as

$$\sigma_{rr}^{(i)} = 2\mu_i \left\{ \frac{\partial^2 \phi_i}{\partial r^2} - \frac{\lambda_i \omega^2}{2\mu_i c_{L_i}^2}\phi_2 + \frac{n}{r^2}\left(r\frac{\partial \psi_i}{\partial r} - \psi_i \right) - k_z \frac{\partial^2 \chi_i}{\partial r^2} \right\} \tag{12}$$

$$\sigma_{r\theta}^{(i)} = 2\mu_i \left\{ \frac{n}{r^2}\left(\phi_i - r\frac{\partial \psi_i}{\partial r} \right) - \frac{\partial^2 \psi_i}{\partial r^2} - \frac{k_{\psi_i}^2}{2}\psi_i + \frac{nk_z}{r^2}\left(r\frac{\partial \chi}{\partial r} - \chi_i \right) \right\} \tag{13}$$

$$\sigma_{rz}^{(i)} = 2\mu_i \left\{ 2k_z \frac{\partial \phi_i}{\partial r} + \frac{nk_z}{r}\psi_i + \left(k_{\psi_i}^2 - k_z^2 \right) \frac{\partial \chi_i}{\partial r} \right\} \tag{14}$$

where $\nabla^2 = \frac{\partial^2}{\partial r^2} + \frac{1}{r}\frac{\partial}{\partial r} + \frac{1}{r^2}\frac{\partial^2}{\partial \theta^2} + \frac{\partial^2}{\partial z^2}$, time dependence has the form $\exp(j\omega t)$ and $c_{L_i} = \sqrt{\frac{\lambda_i + 2\mu_i}{\rho_i}}$ and $c_{T_i} = \sqrt{\frac{\mu_i}{\rho_i}}$ are the compressional and shear wave velocities in the solids, respectively. Applying the method of separation of variables, the solution of the equations for potentials, associated with an axial wave number k_z, radial wave number (k_{ϕ_i}, k_{ψ_i}) and circumferential mode parameter n.

For the torsion mode, the scalar components of the displacement are shown as below, giving the non-vanishing components of displacement and stresses:

$$u_\theta^{(i)} = -\frac{\partial \psi_i}{\partial r},\ \sigma_{r\theta}^{(i)} = -2\mu_i \left\{ \frac{\partial^2 \psi_i}{\partial r^2} + \frac{k_{\psi_i}^2}{2}\psi_i \right\} \tag{15}$$

$$\psi_i = [C_i J_0(k_{\psi_i} r) + D_i Y_0(k_{\psi_i} r)] \sin(k_z z) \exp(j\omega t) \tag{16}$$

While in Equation (15) and Equation (16), the scalar potentials ψ_i and k_{ψ_i} are known as the Helmholtz decomposition. Under that case the boundary conditions become:

$$\begin{aligned}
&\sigma_{r\theta}^{(1)}(r,z) = 0,\\
&u_\theta^{(1)}(r,z) = u_\theta^{(2)}(r,z),\ \sigma_{r\theta}^{(1)}(r,z) = \sigma_{r\theta}^{(2)}(r,z),\\
&u_\theta^{(2)}(r,z) = u_\theta^{(3)}(r,z),\ \sigma_{r\theta}^{(2)}(r,z) = \sigma_{r\theta}^{(3)}(r,z),\\
&\sigma_{r\theta}^{(3)}(r,z) = 0
\end{aligned} \tag{17}$$

Thus the vibration equation $[\mathbf{M}]\{\mathbf{x}\} = \{0\}$ becomes $[\mathbf{T}]\{\mathbf{x}\} = \{0\}$, whereas $[\mathbf{T}]$ is a 7×7 matrix whose components are calculated respectively. In Equation (17), the circumferential displacement $u_\theta^{(i)}$ is independent of θ. $\sigma^{(1)}$ stands for the normal components of the intima stresses, $\sigma^{(2)}$ stands for the normal stress components between the intima and the media, and $\sigma^{(3)}$ stands for the normal stress components between the media and the adventicia.

The other simple kind vibration is longitudinal mode vibration, and under this vibration the motion is confined to the plane perpendicular to the z-axis, which could move, expand and contract within their planes. The solution for the displacement and stress vector is shown as below:

$$u_r^{(i)} = \frac{\partial \phi_i}{\partial r} - k_z \frac{\partial \chi_i}{\partial r} \tag{18}$$

$$u_z^{(i)} = k_z \phi_i + k_{\psi_2}^2 \chi_i \tag{19}$$

$$\sigma_{rr}^{(i)} = \mu_i \left\{ 2\frac{\partial^2 \phi_i}{\partial r^2} - \frac{\lambda_i \omega^2}{\mu_i c_{L_i}^2}\phi_i - 2k_z \frac{\partial^2 \chi_i}{\partial r^2} \right\} \tag{20}$$

$$\sigma_{rz}^{(i)} = \mu_i \left\{ 2k_z \frac{\partial \phi_i}{\partial r} + \left(k_{\psi_i}^2 - k_z^2\right) \frac{\partial \chi_i}{\partial r} \right\} \tag{21}$$

$$\phi_i = [A_i J_0(k_{\phi_i} r) + B_i Y_0(k_{\phi_i} r)] \sin(k_z z) \exp(j\omega t) \tag{22}$$

$$\chi_i = [E_i J_0(k_{\psi_i} r) + F_i Y_0(k_{\psi_i} r)] \cos(k_z z) \exp(j\omega t) \tag{23}$$

Under that case the boundary conditions become:

$$\begin{aligned}
&\frac{\partial p(r,z)}{\partial r} = \rho_f \omega^2 u_r^{(1)}(r,z),\\
&\sigma_{rr}^{(1)}(r,z) = -p(r,z),\ \sigma_{rz}^{(1)}(r,z) = 0,\\
&u_{rr}^{(1)}(r,z) = u_r^{(2)}(r,z),\ u_z^{(1)}(r,z) = u_z^{(2)}(r,z),\\
&\sigma_{rr}^{(1)}(r,z) = \sigma_{rr}^{(2)}(r,z),\ \sigma_{rz}^{(1)}(r,z) = \sigma_{rz}^{(2)}(r,z),\\
&u_{rr}^{(2)}(r,z) = u_r^{(3)}(r,z),\ u_z^{(2)}(r,z) = u_z^{(3)}(r,z),\\
&\sigma_{rr}^{(2)}(r,z) = \sigma_{rr}^{(3)}(r,z),\ \sigma_{rz}^{(2)}(r,z) = \sigma_{rz}^{(3)}(r,z),\\
&\sigma_{rr}^{(3)}(r,z) = \sigma_{rz}^{(3)}(r,z) = 0
\end{aligned} \tag{24}$$

Thus the vibration equation $[\mathbf{M}]\{\mathbf{x}\} = \{0\}$ becomes $[\mathbf{L}]\{\mathbf{x}\} = \{0\}$, whereas $[\mathbf{L}]$ is a 13×13 matrix whose components are calculated respectively. We conducted the simulation based on the above theoretical derivations. The simulation environment was Ansys 16.0, and the

simulation of the normal condition and the varicose veins conditions of the radial vascular vessel were compared and analyzed. In our simulation, the models of normal condition and the varicose veins condition were shown in Figure 2 and Figure 3 respectively. In our simulation modeling for Figure 2 and Figure 3, the geometrical model consists of a three-dimensional axisymmetric tube with a length of L, an inner diameter of R and a wall thickness. We also set E, ν and ρ standing for Young modulus, poison ratio and density. For the boundary condition, we set the outlet pressure as $\Delta p(t) = p(t) - p(t - \Delta t)$ which is calculated from subjects' SBP and DBP values. After we conducted the statistical data arrangement for normal subjects and stenosis subjects, we entered the different data of normal blood pressure and stenosis blood pressure for Figure 2 and Figure 3 respectively. And some other data such as inner diameter and density were also adjusted for stenosis groups in Figure 3.

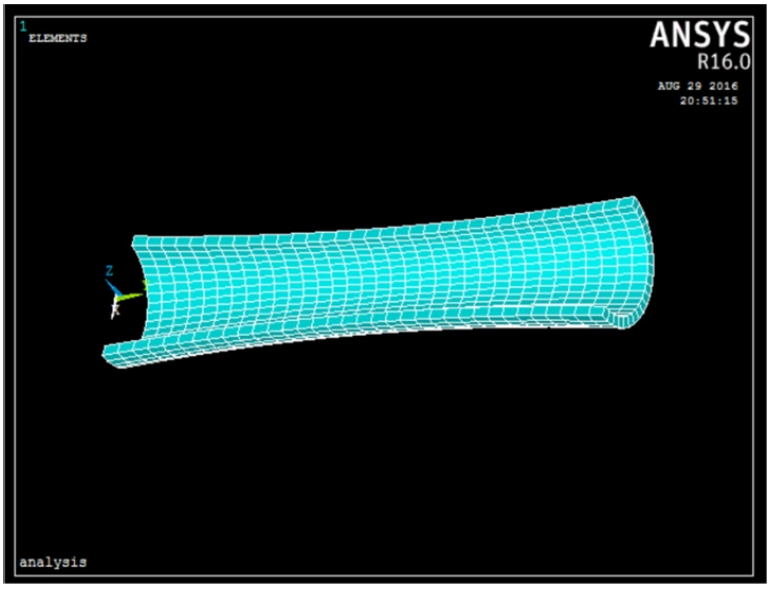

FIGURE 2. The Ansys modeling for radial artery in normal condition

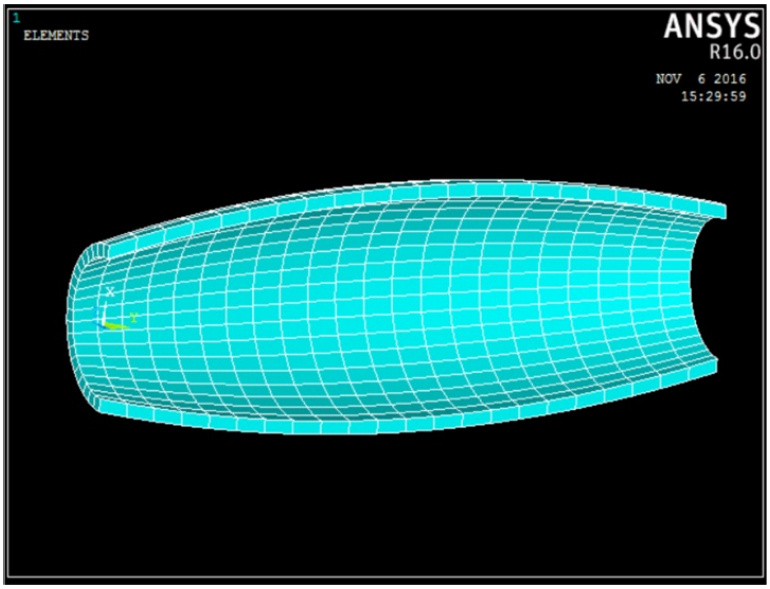

FIGURE 3. The Ansys modeling for radial artery in varicose veins condition

3. **Vibration Analysis.** After we constructed the two models and input all the related parameters, we conducted the vibration modal analysis inside Ansys 16.0, and in our analysis we focused on the first five orders of the normal condition and the varicose veins condition respectively. So we displayed the vibration frequencies and the vibration mode of the first five orders for both conditions. For example, the first to fifth order vibration mode contours of the normal condition are listed in Figure 4, and the vibration frequencies of these five contours are listed in Table 2.

TABLE 2. The vibration frequency of the 1st to 5th vibration mode for normal condition

Number	Vibration Mode	Frequency (Hz)
1	The first-order mode	101.65
2	The second-order mode	103.73
3	The third-order mode	142.12
4	The fourth-order mode	176.19
5	The fifth-order mode	187.99

Similar to the normal condition, we also conducted the first five orders vibration calculation for the varicose veins condition. The first to fifth order vibration contours of the varicose veins condition are shown in Figure 5, and the vibration frequencies of these orders are listed in Table 3.

TABLE 3. The vibration frequency of the 1st to 5th vibration mode for varicose veins

Number	Vibration Mode	Frequency (Hz)
1	The first-order mode	53.166
2	The second-order mode	84.587
3	The third-order mode	105.87
4	The fourth-order mode	122.33
5	The fifth-order mode	125.00

Combining the vibration frequencies of both groups together, we could observe the comparative frequency curves, which are shown in Figure 6. From this comparative curve we could find the vibration frequency of the varicose veins is lower than that of the normal condition at each vibration order. Under the varicose veins condition, the vibration frequency at the 4th or 5th order tends to be stable.

In order to compare with the theoretical analysis, we also conduct experiments for radial artery signals acquisition. A population of 72 subjects between 25 to 85 years old was recruited from a health screen center, and initially measured. All the patients' waveforms were measured and recorded in the exercise intervention clinic of Chinese PLA hospital. These patients mainly came from the north provinces of China, such as Beijing, Shandong, and Shanxi. Subjects with irregular heart rhythm, heart failure, and significant cardiovascular disease were excluded according to the questionnaire. Hypertension is defined as a systolic blood pressure ≥ 140 mmHg, or diastolic blood pressure ≥ 90 mmHg. Our experiment sample included hypertension patients, and details are given in Table 4. Our study focuses on circumstances where varying systolic blood pressure leads to specific radial waveforms characteristics. The systolic blood pressure of the chosen sample therefore ranges widely, with small variations of other factors, such as age, heart rate, and diastolic blood pressure. The hypertension population are all of the condition where systolic blood pressure ≥ 140 mmHg.

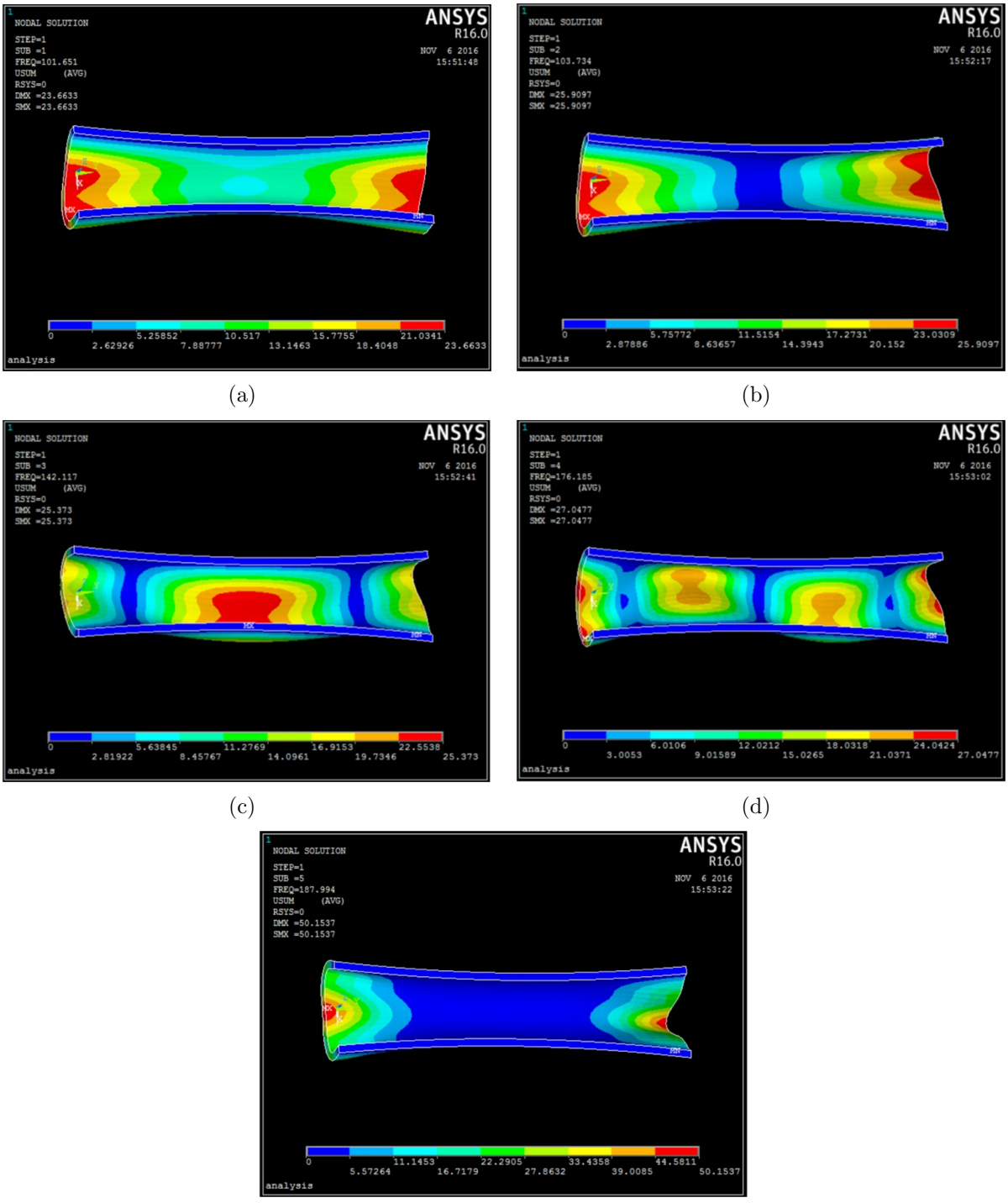

FIGURE 4. The mode contour of radial vascular in normal condition for each vibration mode, the first-order mode (a), the second-order mode (b), the third-order mode (c), the fourth-order mode (d), and the fifth-order mode (e)

All measurements were performed in air-conditioned environments (22-26°C). Each subject rested for at least 10 minutes before measurements. Measurements were taken in a temperature-controlled room between 8:30 and 11:00 AM. All measurements were obtained after 12 h fasting. No consumption of alcohol was allowed for 24 h, and no

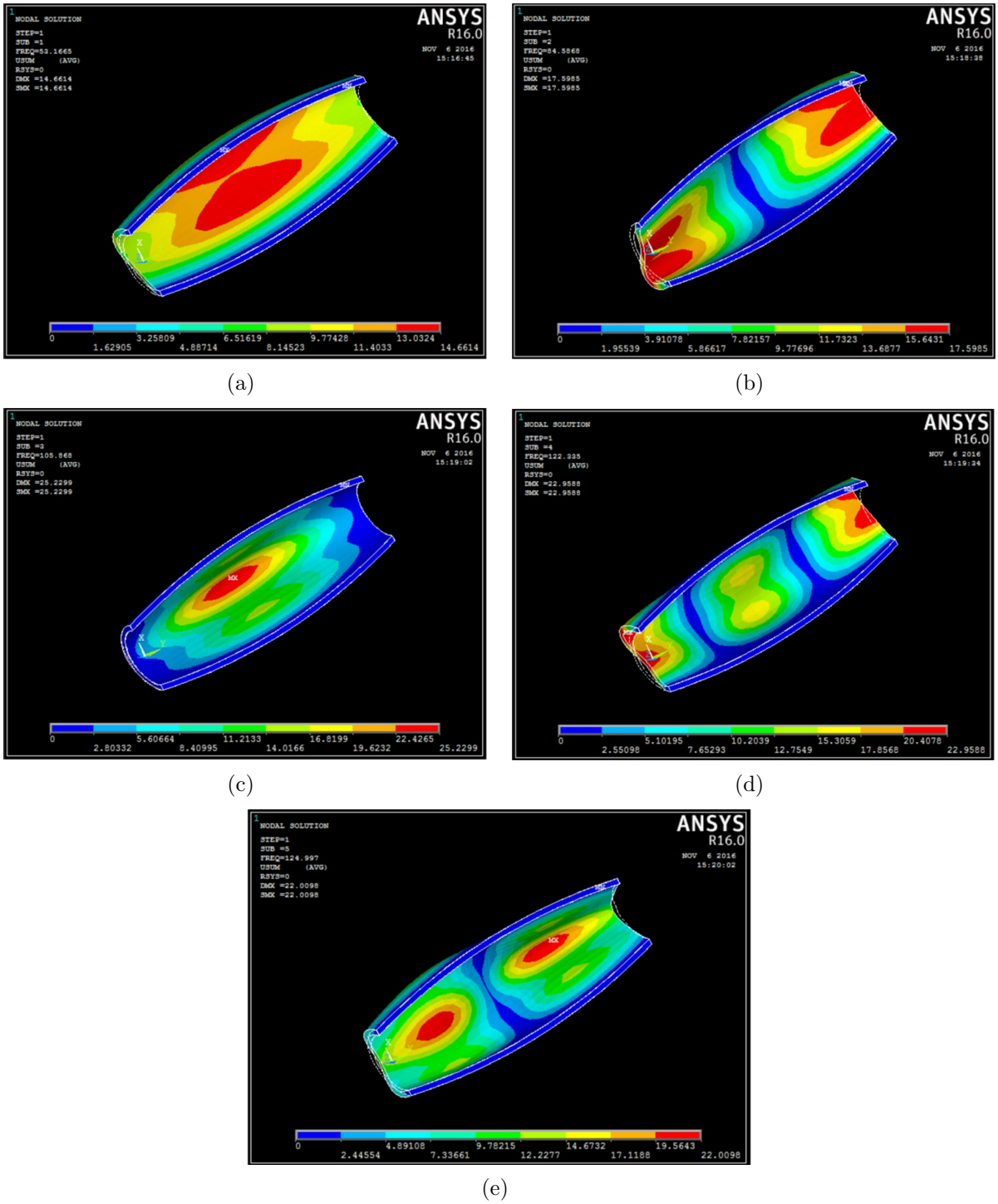

FIGURE 5. The mode contour of radial vascular in varicose veins condition for each vibration mode, the first-order mode (a), the second-order mode (b), the third-order mode (c), the fourth-order mode (d), and the fifth-order mode (e)

tea, coffee, or smoking for 8 h before the examination. For each patient, systolic blood pressure (SBP) and diastolic blood pressure (DBP) were measured three times on the left arm with an Omron HEM-7012 (Omron Healthcare, Japan). Mean arterial pressure was calculated as one third of pulse pressure added to DBP. All measurements were

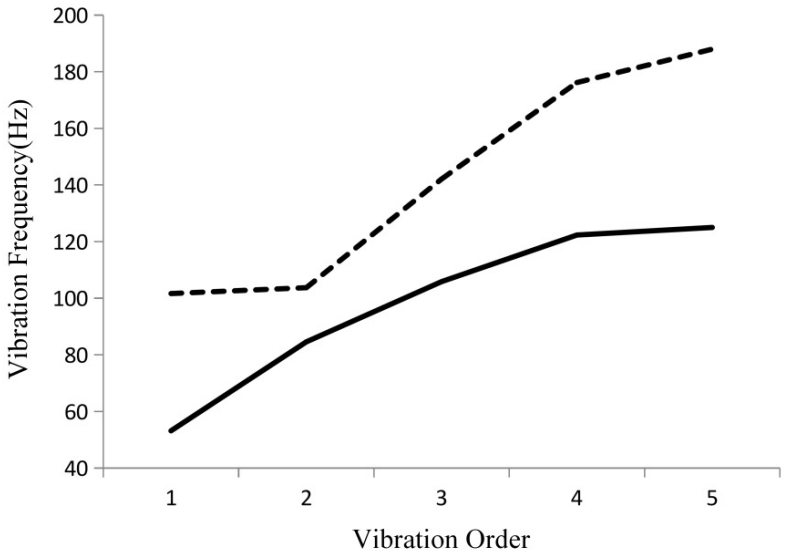

FIGURE 6. The comparative frequency curves for the normal condition and the varicose veins condition for the first five vibration orders. The dotted line stands for the normal condition, and the solid line stands for the varicose veins condition.

TABLE 4. Characteristics of the study populations ($n = 72$)

Characteristics	Mean ± SD	Range
Male	31 (43.1%)	
Hypertension	16 (22.2%)	
Age (years)	51±2.6	24-84
Height (cm)	162.6±7.1	150-180
Weight (kg)	62.6±9.7	40-84
SBP (mmHg)	127.1±23.0	105-158
DBP (mmHg)	73.9±8.4	60-95
HR (beats/min)	70.4±3.8	65-73

performed by the same operator and conducted in the supine position, and recorded by Hu et al. as the measurement reference [14]. Based on the methods and techniques established in the study, we developed arterial stiffness detector (BX-CFTI-200) and noninvasive central arterial pressure analyzer (BX-CAP-100), and demonstrated them in the exercise intervention clinic of Chinese PLA hospital. BX-CAP-100 records radial pulse waveform using applanation tonometry and obtains central arterial pressure waveform by the transformation of GTF. Pulse wave analysis was then applied to extracting a number of hemodynamic indexes [15], including central SBP, AI and SEVR [16]. This equipment has cheap cost and easy to operate, satisfying the requirement of patient waveforms obtainment [17]. After our selection, the initial group was divided into one stenosis group (15 subjects) and the other one control group (57 subjects).

According to the corresponding reference, the complete arterial pulse can be described by 10 harmonics at most, and over 95% of the signal energy could be described in the first 5 to 9 harmonics [18]. The first 4 have been found to reliably estimate central blood pressure signals [19], so we selected this for the transfer function, and found that within the 1-4th to 1-10th harmonics was appropriate. From this transfer function we obtained the matching function of the radial artery waveform, and after residual calculation the

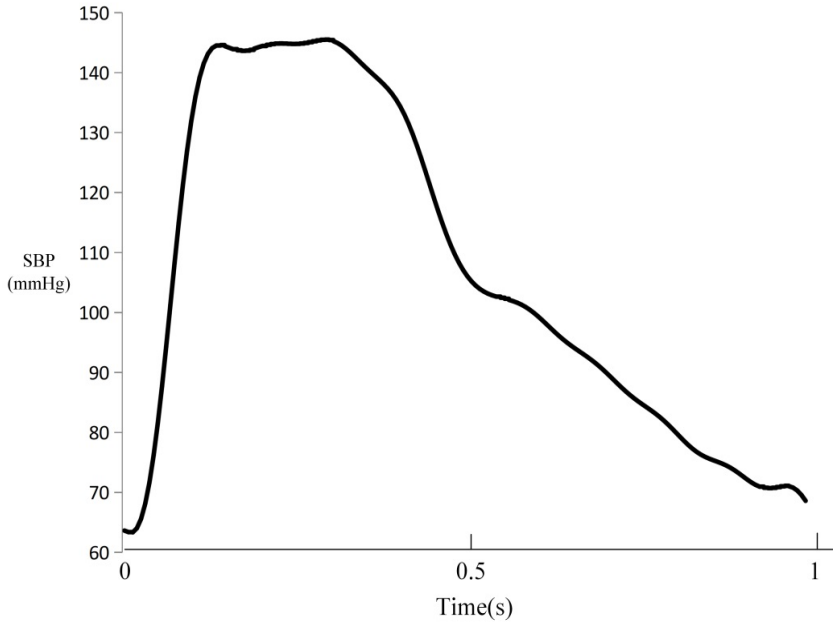

FIGURE 7. The selected average radial waveform of pulse waves within one cycle for stenosis group

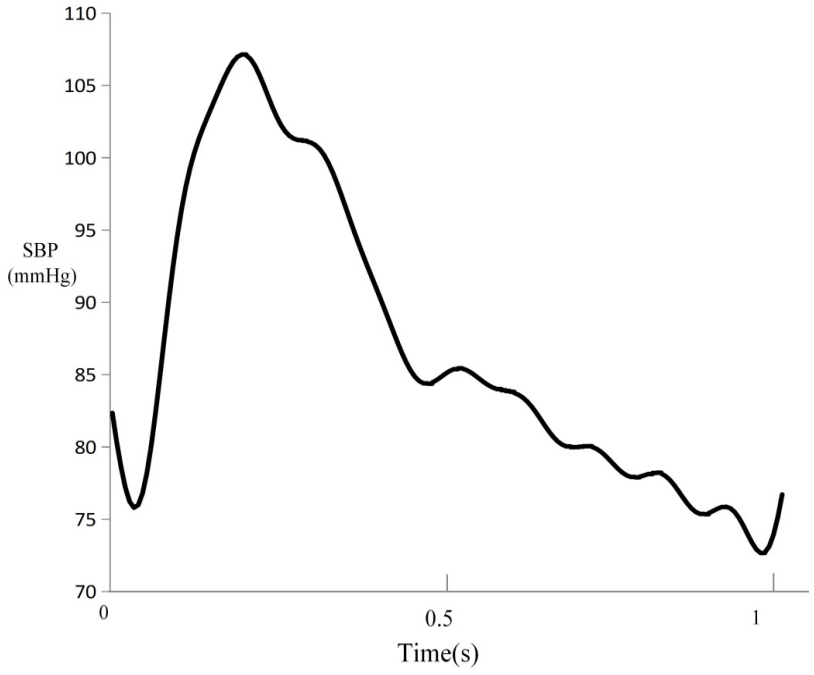

FIGURE 8. The selected average radial waveform of pulse waves within one cycle for the control group

function is confirmed as the combination of 10 harmonics shared with the least residual, shown in Equation (25):

$$P_{G1} = P_0 + P_0 C \left(e^{\omega kt} + e^{2\omega kt} + e^{3\omega kt} + \cdots + e^{8\omega kt} + e^{9\omega kt} + e^{10\omega kt}\right) \tag{25}$$

For the fitting function precision calculation, we first calculated the precision for fitting function within different harmonics numbers [20], and then adjusted the fitting parameters C and k, attempting to obtain the most appropriate parameter with the least residual for

TABLE 5. The comparison of fitting parameter values for the stenosis group and control group

	SBP	C	k
Stenosis Group	155	2.98	0.59
Control Group	135	1.16	0.43

both the stenosis group and the control group. After we conduct the statistical analysis, we could compare the two values between the stenosis group and the control group, which are shown in Table 5.

Above all, we could summarize the main points from the comparison between the stenosis subjects and the control group subjects for both waveforms and parameters. Although the representative waveforms we chose for the stenosis and the control stand for case, we could find that the stenosis affects the waveform shape and leads to larger width of high SBP within one cycle. And the waveform parameters get increased compared to the control group. The experimental results could provide evidence for our former simulation study for stenosis condition. The theoretical vascular vibration analysis provided one important method for revealing the intrinsic implications under the radial pulse waveforms of different subjects [21,22]. Compared to the previous work, our study group developed our specific medical instrument arterial stiffness detector (BX-CFTI-200) and noninvasive central arterial pressure analyzer (BX-CAP-100), and our instrument could obtain the radial waveforms more precisely. Our instrument design conducted waveforms acquisition with the corresponding medical parameters exactly and efficiently. Our cooperation hospital Chinese PLA hospital also provided excellent experimental conditions for us to collect actual waveforms of stenosis groups and normal groups. Our theoretical work also involved the vascular vibration modal analysis and hemodynamics analysis.

4. **Conclusions.** This paper has conducted the vibration frequency analysis and the hemodynamics analysis of a radial artery vascular under the normal condition and the arterial stenosis condition respectively. We used analytic and numerical methods for understanding the mechanism of radial vascular vibration and blood flow inside the vascular vessel. We conducted the mathematical derivations of the radial artery vascular mechanics modeling for vibration analysis and hemodynamics analysis respectively. We conducted the Ansys simulation about vibration frequencies' change along the first five orders from both the normal condition and the arterial stenosis condition, and the frequencies tendencies of two conditions were recorded. The Fluent simulation represented the hemodynamics status considering blood flow for stenosis. We could find the arterial stenosis condition has a higher vibration frequency compared to the normal condition, and the arterial stenosis condition's vibration frequency tends to be stable from the fourth vibration order. The hemodynamics analysis demonstrated that stenosis leads to a radically changing flow velocity and pressure, which coincides with the actually measured radial waveform of the representative stenosis subject. Moreover the experimental results could also give evidence to support the theoretical simulation, as stenosis affects the waveform and leads to enlarged waveform parameters. The stenosis' influences on waveforms have the inherent relationship with the theoretical analysis of vascular mechanical property. In future research the study could be designed to analyze and investigate influences of different diseases on arterial wall and blood-aorta interaction. The theoretical vibration analysis could provide guidance for developing more optimized medical instruments, including arterial stiffness detector and hematology analyzer. On the other side, the more advanced medical instruments would also promote the theoretical field progress of medical

science research. Furthermore, the study would tend to focus on more complex parametric modeling of hemodynamics analysis of vascular artery in future research.

Acknowledgment. The authors sincerely thank research center for information technology of sports and health, institute of intelligent machines, for their system design and data acquisition. This paper's project is supported by the research start-up funding No. GY-Z18166 and the research start-up funding No. GY-Z20045 of Fujian University of Technology.

REFERENCES

[1] B. Fetics, E. Nevo, C.-H. Chen and D. A. Kass, Parametric model derivation of transfer function for noninvasive estimation of central pressure by radial tonometry, *IEEE Transactions on Biomedical Engineering*, vol.46, no.6, pp.698-706, 1999.

[2] K. Takazawa, H. Kobayashi, I. Kojima et al., Estimation of central systolic pressure using late systolic inflection of radial artery pulse and its application to vasodilator therapy, *Journal of Hypertension*, vol.30, no.5, pp.908-916, 2012.

[3] Z. Yang, L. W. Zhang, K. M. Liew and J. L. Yu, Transient analysis of single-layered graphene sheet using the kp-Ritz method and nonlocal elasticity theory, *Applied Mathematics and Computation*, vol.258, pp.489-501, 2015.

[4] P. J. Blanco, S. M. Watanabe and R. A. Feijóo, Identification of vascular territory resistances in one-dimensional hemodynamics simulations, *Journal of Biomechanics*, vol.45, pp.2066-2073, 2012.

[5] M. S. Gohel, D. M. Epstein and A. H. Davis, Cost-effectiveness of traditional and endovenous treatments for varicose veins, *British Journal of Surgery*, vol.97, pp.1815-1823, 2010.

[6] K. H. Lee, J. H. Chung, K. T. Kim, S. H. Lee, H. S. Son, J. S. Jung et al., Comparative study of cryostripping and endovenous laser therapy for varicose veins: Mid-term results, *Korean Journal of Thoracic & Cardiovascular Surgery*, vol.48, no.5, pp.345-350, 2015.

[7] M. A. Muller, D. Mayer, B. Seifert, B. Marincek and J. K. Willmann, Recurrent lower-limb varicose-veins: Effect or direct contrast-enhanced three-dimensional MR venographic findings on diagnostic thinking and therapeutic decision 1, *Radiology*, vol.247, no.3, pp.887-895, 2008.

[8] C. A. Figueroa, I. E. Vignon-Clementel, K. E. Jansen, T. J. R. Hughes and C. A. Taylor, A coupled momentum method for modelling blood flow in three-dimensional deformables arteries, *Computer Methods in Applied Mechanics and Engineering*, vol.195, pp.5685-5706, 2006.

[9] F. Gao, Z. Guo, M. Sakamoto and T. Matsuzawa, Fluid-structure interaction within a layered aortic arch model, *Journal of Biological Physics*, vol.32, no.5, pp.435-454, 2006.

[10] J. F. Gerbeau, M. Vidrascu and P. Frey, Fluid-structure interaction in blood flows on geometries based on medical imaging, *Journal of Biological Physics*, vol.32, pp.155-165, 2005.

[11] L. E. Bergman, K. J. DeWitt, R. C. Fernandez and M. R. Botwin, Effect of non-newtonian behavior on volumetric flow rate for pulsatile flow of blood in a rigid tube, *Journal of Biomechanics*, vol.4, no.3, pp.229-231, 1971.

[12] J. R. Womersley, An elastic tube theory of pulse transmission and oscillatory flow in mammalian arteries, *WADC Technical Report TR*, pp.56-614, 1957.

[13] R. Razaghi, A. Karimi, S. Rahmani and M. Navidbakhsh, A computational fluid-structure interaction model of the blood flow in the healthy and varicose saphenous vein, *Vascular*, vol.24, no.3, pp.254-263, 2016.

[14] F. S. Hu, Y. L. Zhang, Z. C. Ma, Q. Q. Cao, Y. B. Xu, Z. J. He et al., A region-matching method for pulse transit time estimation: Potential for improving the accuracy in determining carotid femoral pulse wave velocity, *Journal of Human Hypertension*, vol.29, pp.675-682, 2015.

[15] M. Peltokangas, A. A. Telembeci, J. Verho, V. M. Mattila, P. Romsi, A. Vehkaoja et al., Parameters extracted from arterial pulse waves as markers of atherosclerotic changes: Performance and repeatability, *IEEE Journal of Biomedical and Health Informatics*, vol.22, no.3, pp.750-757, 2018.

[16] V. Bikia, S. Pagoulatou, B. Trachet, D. Soulis, A. D. Protogerou, T. G. Papaioannou et al., Noninvasive cardiac output and central systolic pressure from cuff-pressure and pulse wave velocity, *IEEE Journal of Biomedical and Health Informatics*, vol.24, no.7, pp.1968-1981, 2020.

[17] V. Bikia, T. G. Papaioannou, S. Pagoulatou, G. Rovas, E. Oikonomou, G. Siasos et al., Noninvasive estimation of aortic hemodynamics and cardiac contractility using machine learning, *Scientific Reports*, vol.10, 15015, 2020.

[18] P. A. Alberto, B. Mark and W. Andrew, Arterial blood pressure measurement and pulse wave analysis – Their role in enhancing cardiovascular assessment, *Physiological Measurement*, vol.31, pp.R1-R47, 2010.

[19] J. E. Sharman, R. Lim, A. M. Qasem, J. S. Coombes, M. I. Burgess, J. Franco et al., Validation of a generalized transfer function to noninvasively derive central blood pressure during exercise, *Hypertension*, vol.47, pp.1203-1208, 2006.

[20] J. Y. Zhu, C. A. Zhu and Y. N. Sun, Theoretical derivation and experimental statistical analysis on radial vascular mechanical modeling within the effects of hypertension, *International Journal of Innovative Computing, Information and Control*, vol.12, no.4, pp.1165-1178, 2016.

[21] H. Dai, X. Liu, P. Hu and J. Liu, A vascular thrombus therapy method based on magnetic-induced vibration, *Bioelectromagnetics*, vol.40, no.6, 2019.

[22] M. A. Armstrong, M. G. Schultz, D. S. Picone, J. A. Black, N. Dwyer, P. R. Thomson et al., Associations of reservoir-excess pressure parameters derived from central and peripheral arteries with kidney function, *American Journal of Hypertension*, vol.33, no.4, 2020.